



Membrane-destabilizing ionizable phospholipids for organ-selective mRNA delivery and CRISPR-Cas gene editing

Shuai Liu^{1,2}, Qiang Cheng^{1,2}, Tuo Wei¹, Xueliang Yu¹, Lindsay T. Johnson¹, Lukas Farbiak¹ and Daniel J. Siegwart¹✉

Endosomal escape remains a fundamental barrier hindering the advancement of nucleic acid therapeutics. Taking inspiration from natural phospholipids that comprise biological membranes, we report the combinatorial synthesis of multi-tailed ionizable phospholipids (iPhos) capable of delivering messenger RNA or mRNA/single-guide RNA for gene editing *in vivo*. Optimized iPhos lipids are composed of one pH-switchable zwitterion and three hydrophobic tails, which adopt a cone shape in endosomal acidic environments to facilitate membrane hexagonal transformation and subsequent cargo release from endosomes. Structure-activity relationships reveal that iPhos chemical structure can control *in vivo* efficacy and organ selectivity. iPhos lipids synergistically function with various helper lipids to formulate multi-component lipid nanoparticles (called iPLNPs) for selective organ targeting. Zwitterionic, ionizable cationic and permanently cationic helper lipids enable tissue-selective mRNA delivery and CRISPR-Cas9 gene editing in spleen, liver and lungs (respectively) following intravenous administration. This rational design of functional phospholipids demonstrates substantial value for gene editing research and therapeutic applications.

The clustered regularly interspaced short palindromic repeat/CRISPR-associated protein 9 (CRISPR-Cas9) technology is a promising therapeutic modality for correction of DNA mutations that cause genetic diseases^{1–6}. Systemic delivery of CRISPR-Cas cargoes using non-viral materials has attracted increasing attention because the transient nature confers increased safety over viral delivery and allows repeat dosing^{7–9}. However, efficacious and safe *in vivo* gene editing using synthetic nanoparticles remains challenging, particularly due to low endosomal escape. So far, there has been a major focus on developing cationic lipids for RNA delivery^{10–13}, with little attention to the critical roles played by zwitterionic phospholipids. Although phospholipids mimic biological membranes, aid RNA encapsulation and are powerful at the membrane fusion step critical for endosomal escape^{14,15}, their chemical architectures are limited by lack of flexibility, such as pH response and tail number alteration. Inspired by biological membranes, we developed a class of pH-switchable, multi-tailed ionizable phospholipids (iPhos) with endosomal membrane destabilization and determined the underlying mechanisms of iPhos-mediated mRNA delivery and CRISPR-Cas9 gene editing.

Phospholipids are distributed throughout nature, serve as the key components of biological membranes and organelles, and are involved in cellular transport pathways^{16,17}. Because even the most effective carriers, including FDA-approved DLin-MC3-DMA lipid nanoparticles (LNPs), can only mediate 1–4% of RNA release into the cytoplasm, endosomal escape remains as the most daunting step for delivery^{18–20}. Phospholipids represent an exciting opportunity to overcome a critical limitation of current carriers by inserting into naturally occurring membranes to enhance endosomal escape. Nonetheless, chemical pursuit of lipid structures to access the key physicochemical requirements to facilitate endosomal escape has been severely hampered by limitations in both reac-

tions to access phospholipids and their inherently limited structural flexibility. For instance, the most commonly used phospholipids, 1,2-distearoyl-sn-glycero-3-phosphocholine (DSPC)²¹ and 1,2-dioleoyl-sn-glycero-3-phosphoethanolamine (DOPE)^{22–24} possess constant one irreversible zwitterion (at least in organisms) and two hydrophobic tails, lacking chemical handles to manipulate. To enrich the diversity of phospholipids, well-tailored structures are demanded from rational chemical design.

Inspired by cationic lipid designs, we proposed that integration of their advantages (for example, ionizable amines and multiple alkyl chains) into phospholipid designs with membrane integration potential would dramatically improve the resulting functionality. First, an ionizable reversible zwitterion between neutral physiological environment and acidic endosomal compartment might enable pH-triggered membrane rupture. Second, one small zwitterion head combined with over two hydrophobic tail body would adopt a cone shape more easily, inducing a strong trend of membrane phase transformation. To realize these assumptions and design multi-functional phospholipids, ring-opening of dioxaphospholane oxide molecules provides a way forward. These molecules are capable of conjugating with primary, secondary and tertiary amines, such that controllable hydrophobic tail numbers and pH-switchable zwitterions can be realized through this modular synthetic strategy. Until now, most vehicles only demonstrate efficacy in liver hepatocytes^{15,25,26}, and delivery outside the liver is a major need for future correction of genetic diseases. Following optimization of material architecture, we discovered that the resulting iPhos lipids enabled establishment of structure-selectivity relationships to further define mechanisms for extrahepatic delivery. Development of tissue-selective carriers is of great importance to minimize side effects and enable targeting of cell types required for treatment of genetic diseases.

¹The University of Texas Southwestern Medical Center, Department of Biochemistry, Simmons Comprehensive Cancer Center, Dallas, TX, USA. ²These authors contributed equally: Shuai Liu, Qiang Cheng. ✉e-mail: Daniel.Siegwart@UTSouthwestern.edu

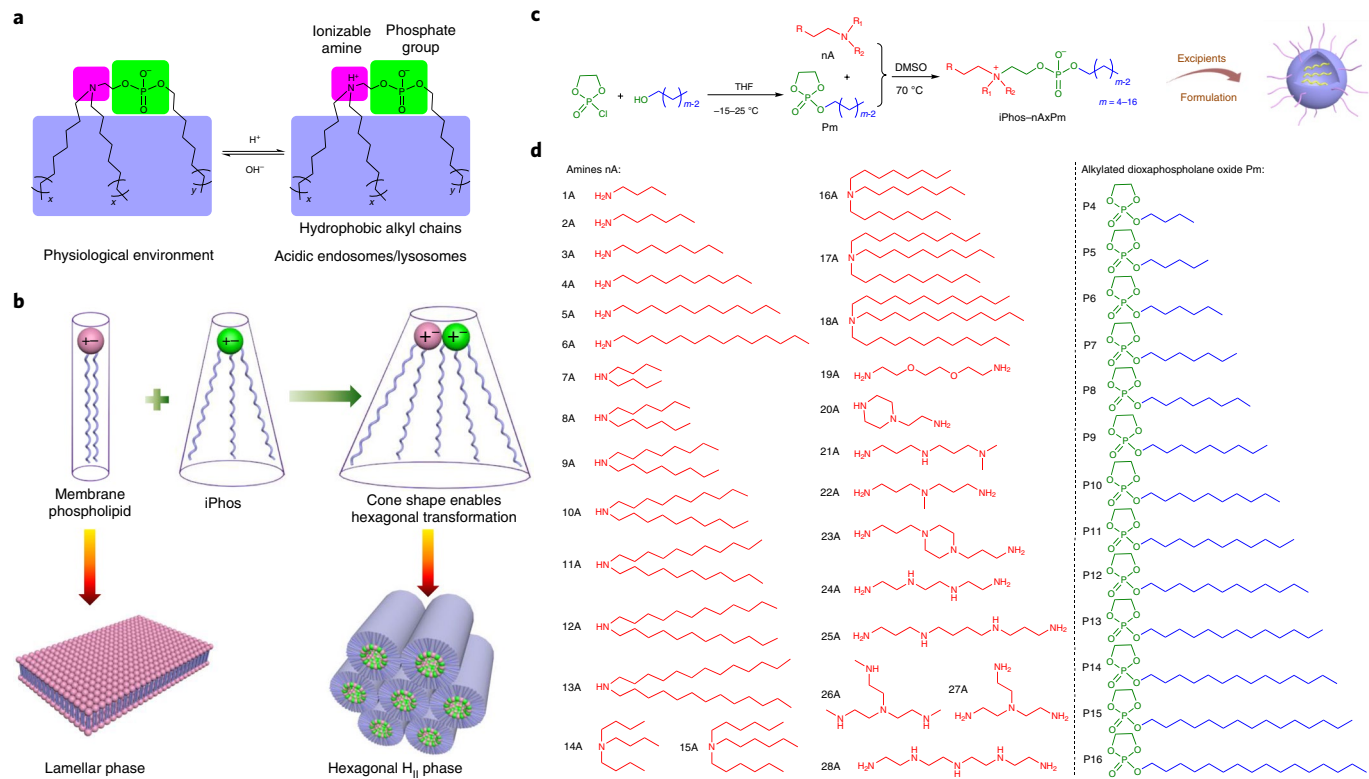


Fig. 1 | A combinatorial library of iPhos lipids was chemically synthesized and studied, which led to the elucidation of a physical mechanism of action for enhanced endosomal escape. **a**, Efficacious iPhos lipids were composed of one ionizable amine, one phosphate group and three hydrophobic alkyl tails. On entering acidic endosomes/lysosomes, protonation of the tertiary amine induced a zwitterionic head group, which could readily insert into membranes. **b**, Most biological membrane phospholipids possess a zwitterion and adopt a lamellar phase. When iPhos lipids were mixed and inserted into the endosomal membranes, the formed cone shape by small ion pair head and multiple hydrophobic tails enabled hexagonal transformation. **c**, Synthetic routes of iPhos: alkylated dioxaphospholane oxide molecules (Pm) were conjugated to amines (nA) to obtain iPhos (nAxPm). ‘x’ in ‘nAxPm’ indicates the number of Pm molecules modified on one amine molecule. **d**, A list of 28 amines and 13 alkylated dioxaphospholane oxide molecules used for iPhos synthesis.

Taking inspiration from natural phospholipids that comprise biological membranes and mediate transport in cells, we report the combinatorial synthesis of 572 iPhos lipids capable of delivering mRNA or mRNA/sgRNA for gene editing *in vivo* via bio-inspired mechanisms. Following initial evaluation, iPhos lipids (7A1P4–13A1P16) containing one tertiary amine, one phosphate group and three alkyl tails enabled the highest protein expression. The pH-switchable small zwitterion head and multiple tails aided endosomal membrane fusion and hexagonal phase transformation. Structure–activity relationships (SAR) revealed that tail length of iPhos lipids affected both *in vivo* efficacy and organ selectivity. In terms of LNP designs, iPhos lipids are functional and represent the important core component in the reported delivery systems. First, top-performing iPhos 9A1P9 exhibited 40- to 965-fold higher *in vivo* efficacy compared to previous benchmarks DOPE and DSPC. Second, 9A1P9 demonstrated universal applicability to synergistically function with zwitterionic, ionizable cationic and permanently cationic helper lipids to formulate multi-component LNPs for selective organ targeting (SORT)²⁷ to mediate exclusive transfection in spleen, liver or lungs. This phenomenon is of vital importance for the treatment of various tissue-specific diseases. The best 9A1P9-5A2-SC8 and 9A1P9-DDAB formulations mediated high mRNA expression and CRISPR–Cas9 gene editing specifically in liver and lung, respectively. We believe the rationally designed iPhos and *in vivo* SAR expand nanomaterial development to further the fields of gene delivery and editing and present translational potential to realize clinical applications.

Results

Rational design of iPhos for superior endosomal escape. In the past decade, substantial efforts have established four-component LNP systems for RNA delivery, which are composed of cationic ionizable lipids, phospholipids, cholesterol and poly(ethylene glycol) (PEG) lipids^{28,29}. Our previous work demonstrated that phospholipids assist mRNA loading into LNPs⁸, and increasing phospholipid content can improve delivery efficacy¹⁴. Furthermore, phospholipids show similarity to biological membranes, and might enable membrane fusion readily. However, phospholipids do not natively possess a pH switch that has been shown to be essential to mediate LNP disruption and endosomal membrane fusion following cellular uptake and pH acidification in endosomes^{11,30}. Moreover, phospholipid species and architectures are limited to date, where common phospholipids (for example, DSPC and DOPE) typically possess one irreversible zwitterion and two hydrophobic tails that lack the chemical features to alter shape within endosomes to address the daunting escape requirements. Previously, cationic lipids have been extensively explored^{28–31} and integrating their advantages (for example, ionizable amines and multiple tails) to phospholipids represents an opportunity to tailor the structures of phospholipids. For this purpose, we rationally designed iPhos lipids, which contained an ionizable amine, a phosphate group and three hydrophobic tails. The small zwitterion constituted by amine and phosphate group is predicted to be reversible at different pHs. At physiological pH (roughly 7.4), the tertiary amine group will not be protonated and the negatively charged iPhos will have difficulty fusing into the membranes. In contrast, on entering the acidic endosomes, the

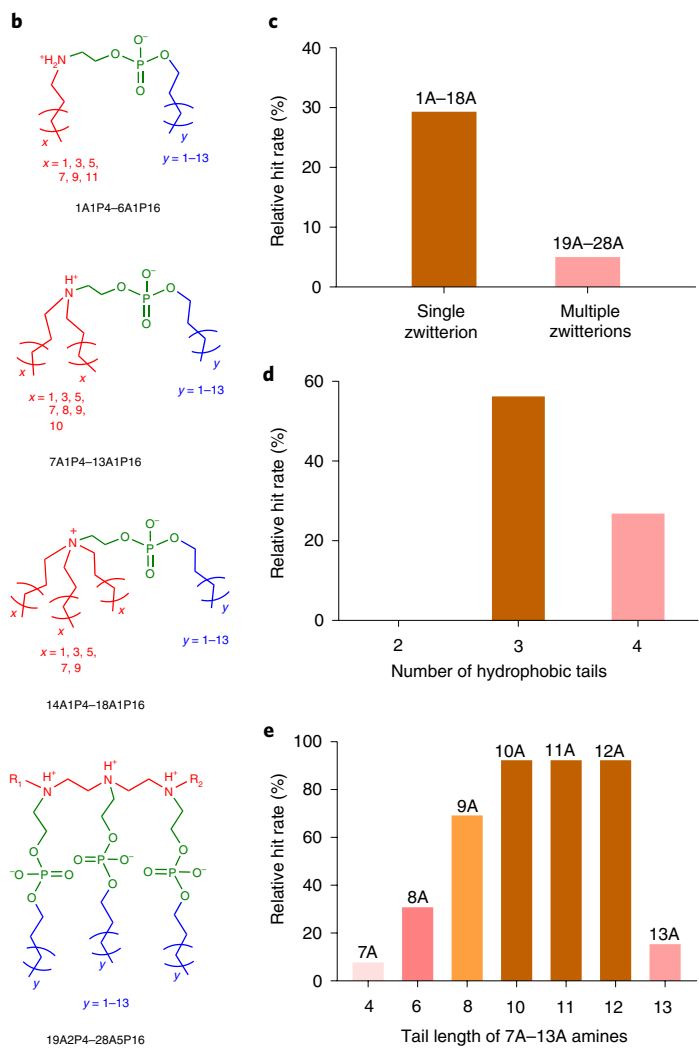
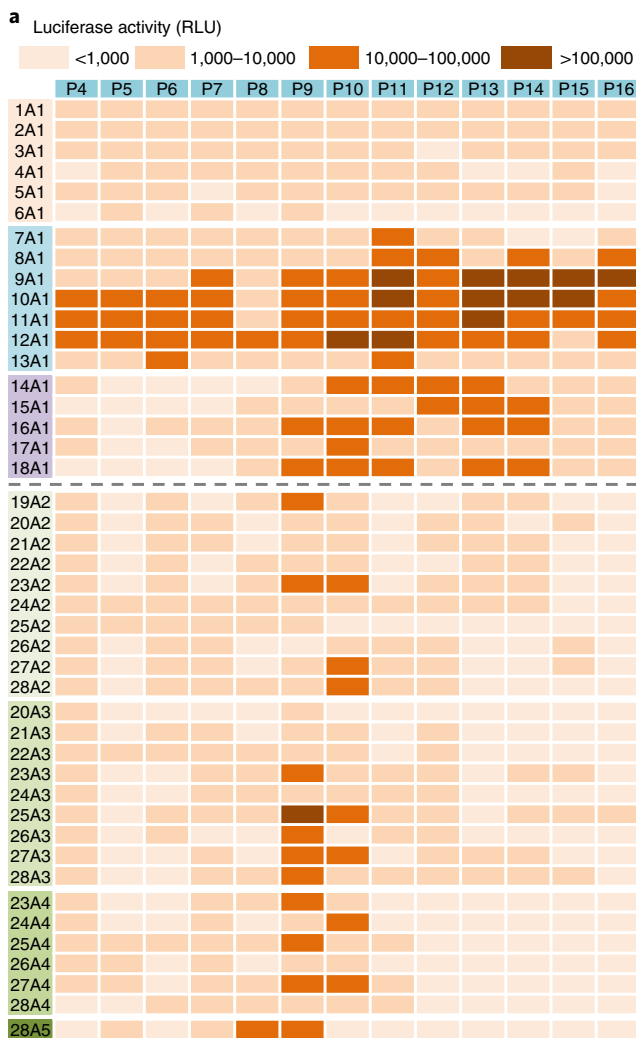


Fig. 2 | SAR of iPhos lipids for luciferase mRNA delivery in vitro. **a**, A heat map of luciferase expression following treatment of IGROV1 cells with iPLNPs (50 ng firefly luciferase (Fluc) mRNA, $n=3$ biologically independent samples). Relative light units (RLU) of $>10,000$ was counted for the hit rate calculation. **b**, Representative chemical structures of iPhos with different numbers of zwitterions and tails in an acidic endosomal environment. **c**, The relative hit rate of iPhos with a single zwitterion and multiple zwitterions. **d**, The relative hit rate of iPhos (1A1P4–18A1P16) with a single zwitterion and different numbers of tails. **e**, Among the efficient iPhos (7A1P4–13A1P16), tail length of starting amines influenced the ultimate in vitro efficacy.

tertiary amine will be protonated to form a zwitterionic head (Fig. 1a). On studying the substrate scope, we found that the three hydrophobic tail body was easier to mediate membrane phase transformation than that of two chains. The mechanism of action, therefore, is different from that of classic gene carriers, because synthetic iPhos lipids can overall insert into natural phospholipid membranes, with preferable small ion pairs coupled with large tail body adopting a cone shape, to facilitate hexagonal II (H_{II}) phase formation (Fig. 1b).

To overcome previous limitations in synthetic routes, we focused on ring-opening reactions^{32,33} that could yield diverse products with chemical complexity to meet the aforementioned design guidelines. The combinatorial reaction of amines (nA) with alkylated dioxaphospholane oxides (Pm) yielded 572 iPhos lipids (termed nAxPm) (Fig. 1c) where 'x' indicates the number of Pm molecules modified on one amine molecule. Pm molecules were synthesized via esterification of 2-chloro-2-oxo-1,3,2-dioxaphospholane (COP) from corresponding alcohols with different alkyl chain lengths (Supplementary Fig. 1). Primary, secondary and tertiary amine groups could all trigger Pm ring-opening to introduce different zwitterions (Supplementary Fig. 2). To control the hydrophobic tail and zwitterion numbers, amines with different alkyl chain

and amine group numbers were used (Fig. 1d and Supplementary Fig. 3). The chemical design of iPhos is unique, because zwitterion species (pH switchable and irreversible) become available in addition to group numbers through this strategy, greatly broadening the architectures and varieties of phospholipids.

Top iPhos possessed a pH-switchable head and three tails. To evaluate the potential for mRNA delivery, iPhos LNPs (iPLNPs) were used to transfect ovarian cancer cells IGROV1. iPhos, helper lipid, cholesterol and 1,2-dimyristoyl-rac-glycero-3-methoxy(poly(ethylene glycol-2000)) (DMG-PEG2000) (25:30:30:1 mol/mol) were mixed with mRNA to formulate iPLNPs using the ethanol dilution method. A structurally simple lipid, *N*-methyldioctadecylamine (MDOA), was first used as the helper lipid to demonstrate the iPhos function in the initial screen. iPLNPs can thus be considered a remix of traditional LNPs, where the modular emphasis is placed instead on the zwitterionic (functionally active iPhos) lipid and all other lipids become helper lipids. All initial iPhos lipids exhibited low toxicity (Supplementary Fig. 4). From the in vitro screening heat map, iPhos with a single zwitterion (1A1P4–18A1P16) showed higher mRNA efficacy than that of multiple zwitterions (19A2P4–28A5P16)

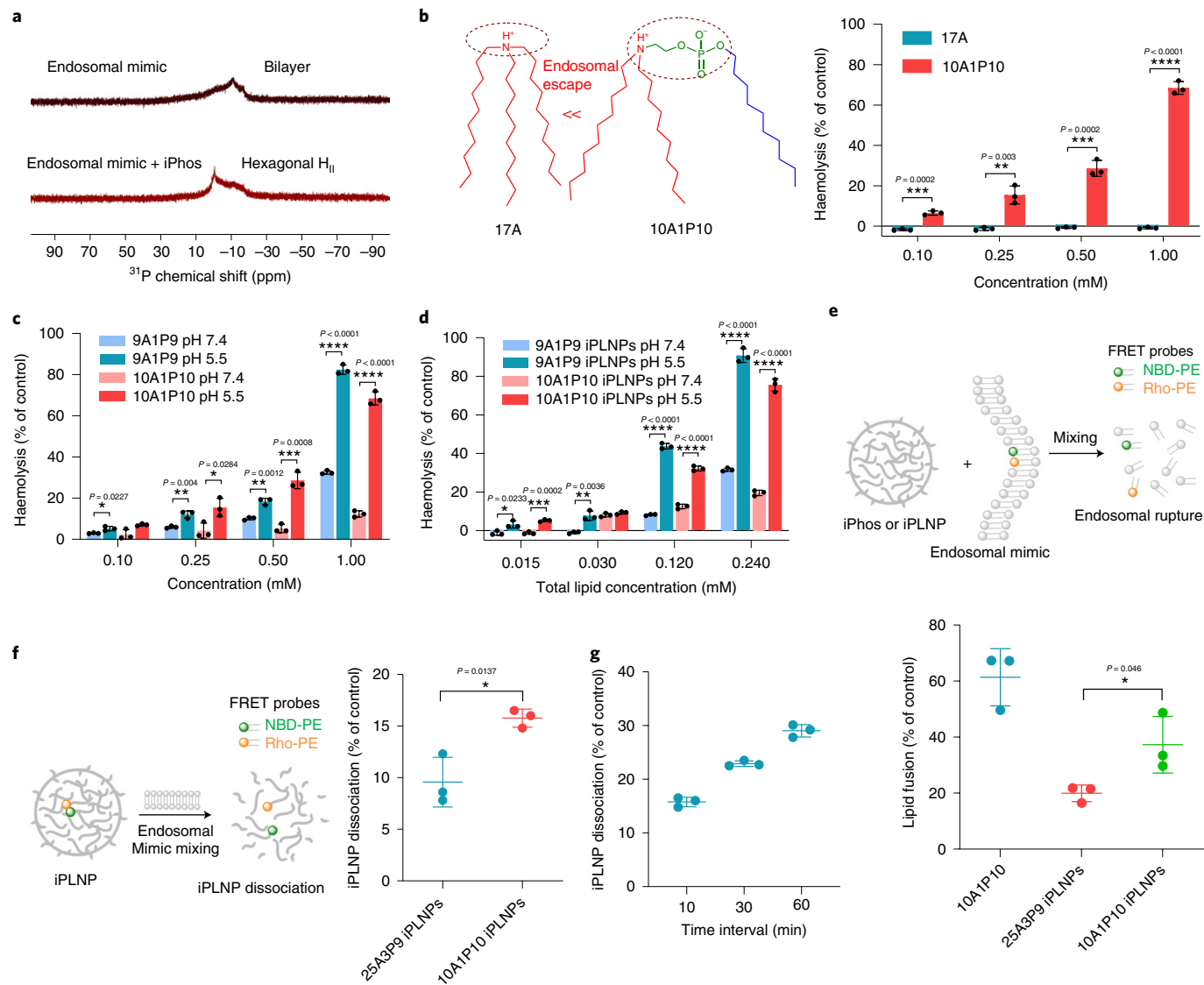


Fig. 3 | Model membrane studies of endosomal escape demonstrated the mechanism of iPhos lipid-mediated RNA delivery with correlation to chemical structure. **a**, ^{31}P NMR spectra of endosomal mimic and a mixture of endosomal mimic with iPhos 9A1P9. iPhos lipid mixing induced membrane hexagonal H_{II} transformation. **b**, Haemolysis of 17A and 10A1P10 at pH 5.5. The zwitterion could notably benefit the endosomal escape. **c**, Haemolysis of 9A1P9 and 10A1P10 at different pHs. **d**, Haemolysis of iPLNPs at different pHs. **e**, Lipid fusion and membrane rupture of 10A1P10 and iPLNPs were determined by a FRET assay at pH 5.5. **f**, iPLNP dissociation by FRET characterization after mixing with anionic endosomal mimics for 10 min at pH 5.5. A single zwitterion showed higher lipid fusion and iPLNP dissociation efficacy than multiple zwitterions. **g**, 10A1P10 iPLNP dissociation at different time intervals at pH 5.5. Data in **b–g** are presented as mean \pm s.d. ($n=3$ biologically independent samples). Statistical significance was analysed by the two-tailed unpaired t-test: **** $P < 0.0001$; *** $P < 0.001$; ** $P < 0.01$; * $P < 0.05$.

(Fig. 2a–c). The reason was that multiple zwitterions constructed a larger head, making it difficult for membrane phase transformation. To further explore the SAR of iPhos with a single zwitterion, two-tailed materials (1A1P4–6A1P16) exhibited far less efficacy, because the small tail body failed to formulate the cone shape with natural membrane phospholipids. iPhos 14A1P4–18A1P16 possessed a permanent zwitterion and lacked structural flexibility on endosomal internalization. iPhos (7A1P4–13A1P16) composed of one tertiary amine, one phosphate group and three hydrophobic tails showed the highest mRNA delivery efficacy as expected, with a hit rate around 60% (Fig. 2d). The small zwitterion head and large tail body promoted membrane fusion and phase transformation from lamellar to hexagonal H_{II} . Among these iPhos lipids, amine tail length was very important and the hit rates of 10–12 chain lengths reached up to 92% (Fig. 2e). These observations are in

contrast to previously reported ionizable amino lipid and lipidoid libraries, where efficacy generally correlated with polyamine cores and higher numbers of alkyl tails^{13,34,35}. These results indicate that iPhos lipids may operate by a different mechanism than ionizable amino lipids do. Next, selected top iPhos lipids (9A1P9, 9A1P15, 10A1P10 and 10A1P16) were purified (Supplementary Fig. 5–8), and the resulting iPLNPs showed appropriate particle sizes (roughly 150 nm) for endocytosis, slightly negative surface zeta potentials (roughly -5 mV) for serum protein resistance, as well as suitable pK_a (6.0–6.5) for in vivo assays (Supplementary Figs. 9 and 10). These capabilities impart synthetic iPhos lipids great potential for in vivo applications.

Model membrane studies of iPhos-mediated endosomal rupture. Although numerous gene delivery systems have been developed^{36–39},

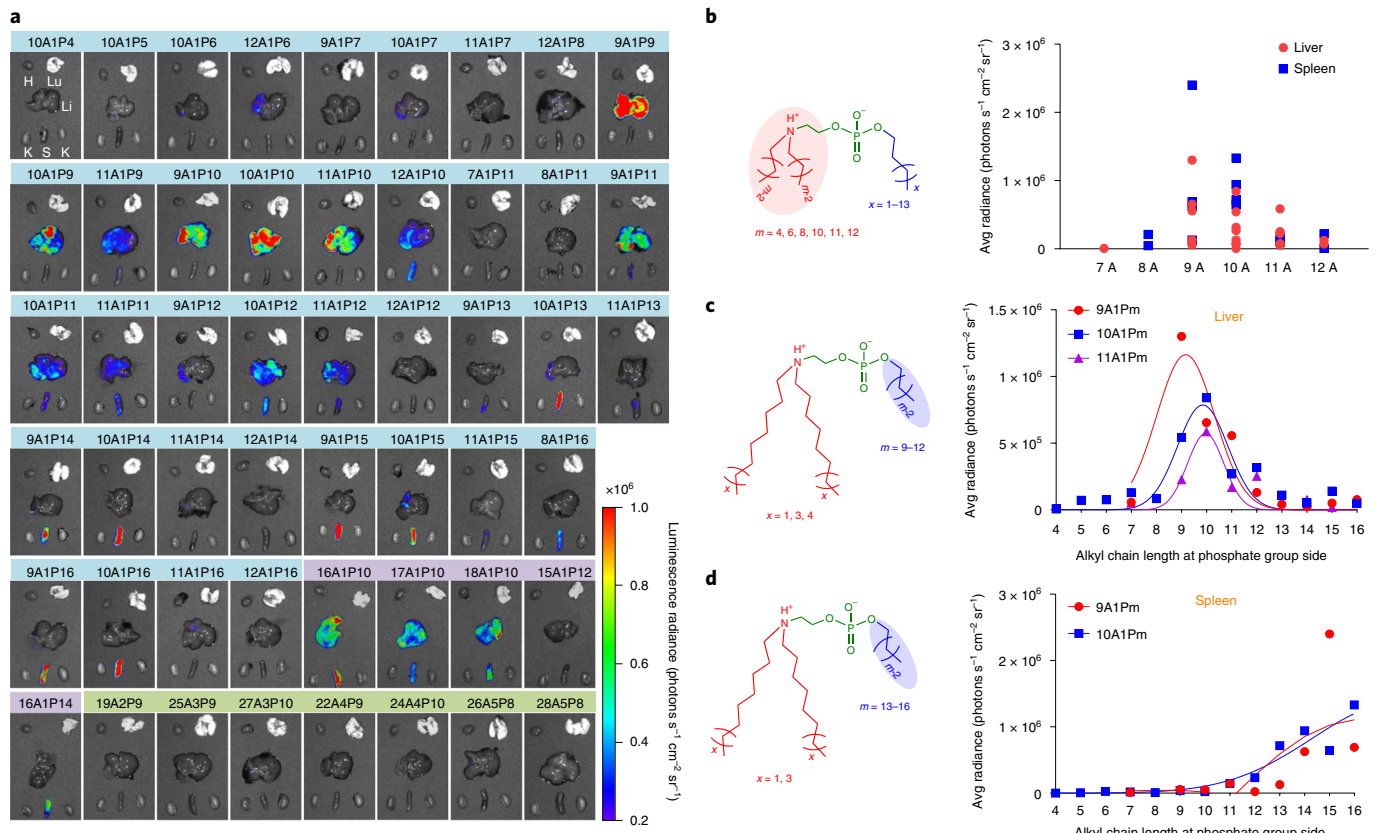


Fig. 4 | Structure-activity studies revealed that iPhos lipid structure controlled in vivo efficacy and organ selectivity. **a**, In vivo evaluation of 51 iPhos at a low Fluc mRNA dose (0.1 mg kg^{-1}). Bioluminescence images of various organs were recorded 6 h after i.v. injection of iPLNPs into C57BL/6 mice. H, heart; Lu, lung; Li, liver; K, kidney; S, spleen. **b**, Among the efficacious 10A1P4–12A1P16 iPhos, hydrophobic chain length at the amine side notably influenced the in vivo mRNA delivery efficacy as quantified by average (avg) radiance. **c**, mRNA expression in liver by iPhos with different alkyl chain length at phosphate group side. Carbon lengths of 9–12 were the most efficient. **d**, mRNA expression in spleen by iPhos with different alkyl chain length at phosphate group side. Alkyl chain lengths of 13–16 were the most efficient.

chemical designs have largely rested on cationic amines with limited pursuit of physical membrane disruption. To verify our hypothesis behind efficacious mRNA delivery, we investigated phase transformation using established ^{31}P NMR spectroscopy techniques^{11,40,41}. Endosomal mimicking liposomes adopted a bilayer structure, as evidenced by the low field shoulder. On mixing with iPhos lipids, the peak asymmetry was reversed and the liposomes transformed to the hexagonal phase (Fig. 3a). Next, the membrane-disruptive activity of iPhos lipids and iPLNPs was evaluated by a haemolysis model^{30,42}. As expected, 10A1P10 with a pH-switchable zwitterion exhibited dramatically higher haemolysis than 17A with a simple tertiary amine, validating the superiority of zwitterion in membrane fusion and rupture (Fig. 3b). Also, 9A1P9, 10A1P10 and related iPLNPs showed higher membrane-disruptive activity at the acidic endosomal compartment compared to that of neutral pH (Fig. 3c,d). The high haemolysis was not due to cytotoxicity (Supplementary Fig. 11).

Following this, a fluorescence resonance energy transfer (FRET) assay was used to evaluate iPhos lipid membrane fusion and iPLNP dissociation. Two DOPE-conjugated FRET probes, 7-nitrobenzo-2-oxa-1,3-diazole (NBD-PE) and lissamine rhodamine B (Rho-PE), were formulated into a single endosomal mimicking liposome, leading to attenuated NBD fluorescence because of FRET to rhodamine. Once lipid fusion occurred, the resulting larger distance between the two probes gave rise to NBD signal increase^{43,44}. 10A1P10 iPLNPs exhibited higher lipid fusion than 25A3P9 iPLNPs, demonstrating that a small single zwitterion

head showed a stronger trend to insert and destroy endosomal membranes compared to that of multiple zwitterions (Fig. 3e). Additionally, 10A1P10 iPLNPs were easier to disassemble to release mRNA than 25A3P9 iPLNPs once mixing with endosomal mimicking liposomes (Fig. 3f,g). These results demonstrate that apart from a large tail body, a pH-switchable small zwitterion head in iPhos lipids is essential for endosomal escape.

iPhos structure-controlled efficacy and organ selectivity. Due to the additional barriers for in vivo delivery, not all carriers with in vitro activity translate to animal models^{45,46}. Moreover, comparing small interfering RNAs/micro RNAs (18–22 bp) to long mRNAs (1,000–6,000 nt), weaker electrostatic association is required, allowing for mRNA release post cellular internalization¹⁴. Therefore, the chemistry of iPhos lipids may have an inherent advantage over cationic lipids and play a pivotal role in mRNA delivery systems.

We selected 51 efficient iPhos lipids from the in vitro screen and evaluated in vivo delivery at a low mRNA dose (0.1 mg kg^{-1}) (Fig. 4a). As expected, iPhos lipids containing multiple zwitterions failed to deliver mRNA in vivo. Further establishing SAR, iPhos lipids with one tertiary amine, one phosphate group and three alkyl tails were the most efficacious. Alkyl chain length greatly affected efficacy and organ selectivity. The chain length at the amine side determined efficacy, and eight to ten carbon lengths mediated high in vivo mRNA expression (Fig. 4b and Supplementary Fig. 12). Alkyl length next to the phosphate group influenced organ selectivity (Fig. 4c,d). Shorter chains (9–12 carbons) showed mRNA translation

in liver, while longer chains (13–16 carbons) would transfer protein expression to spleen. In vivo assessment of 10A1P4–10A1P16 also clearly supported this inference (Supplementary Fig. 13). Next, nanoparticle size, zeta potential and pK_a of these iPLNPs were evaluated, where no obvious differences were observed (Supplementary Fig. 14). At a higher mRNA dose (0.25 mg kg^{-1}), organ selectivity was still achieved (Supplementary Figs. 15 and 16). While we speculate the organ selectivity relates to the chemical structure of mRNA carrier materials⁴⁷, detailed mechanistic studies are still on-going. The SAR provides a guideline to develop other efficacious vector materials with organ selectivity and specificity.

iPLNPs mediated tissue-selective gene delivery and editing.

To confirm that iPhos 9A1P9 was the most important and active component of iPLNPs, we conducted a series of experiments. First, 9A1P9 exhibited 40- to 965-fold higher in vivo efficacy compared to the best currently used phospholipids DOPE and DSPC (Fig. 5a–c). Second, a variety of other established lipids were assessed in our 9A1P9 iPLNP mRNA delivery system as helper lipids to show the broad applicability. We investigated zwitterionic lipids (DOPE), ionizable cationic lipids (MDOA, 1,2-dioleoyl-3-dimethylammonium-propane (DODAP) and 5A2-SC8, ref. ³⁵) and permanently cationic lipids (dimethyldioctadecylammonium bromide salt (DDAB) and 1,2-dioleoyl-3-trimethylammonium-propane (DOTAP)) as helper lipids (Supplementary Fig. 17). The molar ratios of compositions were determined by orthogonal design methodology^{14,48} and shown in Supplementary Table 1. All formulated iPLNPs exhibited appropriate diameters, zeta potentials, mRNA binding, pK_a and high in vitro mRNA delivery efficacy (Supplementary Fig. 18).

We next investigated whether iPhos could be used for SORT^{27,49}. Encouragingly, 9A1P9 iPLNPs with zwitterionic, ionizable cationic, and permanently cationic helper lipids enabled selective mRNA expression in spleen, liver, and lungs, respectively (Fig. 5d–i). Two highly efficacious formulations were further studied and in vivo biodistribution results revealed that spherical 9A1P9-5A2-SC8 and 9A1P9-DDAB iPLNPs mediated high accumulation in liver and lung, respectively (Supplementary Figs. 19 and 20). Since iPhos lipids can enhance already efficacious formulations in a modular fashion, we determined that 9A1P9-5A2-SC8 and 9A1P9-DDAB combinations exhibited high mRNA expression in liver (roughly $10^8 \text{ photons s}^{-1} \text{ cm}^{-2} \text{ sr}^{-1}$, 0.05 mg kg^{-1}) and lung (roughly $10^8 \text{ photons s}^{-1} \text{ cm}^{-2} \text{ sr}^{-1}$, 0.25 mg kg^{-1}), respectively (Fig. 5f–i and Supplementary Fig. 21). Acknowledging that DLin-MC3-DMA (used in FDA-approved Onpattro) LNPs were optimized for siRNA⁵⁰ and not mRNA delivery, DLin-MC3-DMA LNPs provide value as a reference^{15,51}. Comparing to this established formulation, 9A1P9-5A2-SC8 iPLNPs showed 13-fold higher mRNA delivery efficacy than DLin-MC3-DMA LNPs in vivo (Fig. 5j,k and Supplementary Fig. 22). Therefore, iPLNPs are different from traditional cationic

lipid LNPs, and high efficacy and controllable organ selectivity are both accomplished. Kinetic analysis revealed that protein expression occurred rapidly and peaked at around 6 h post injection (Supplementary Fig. 23).

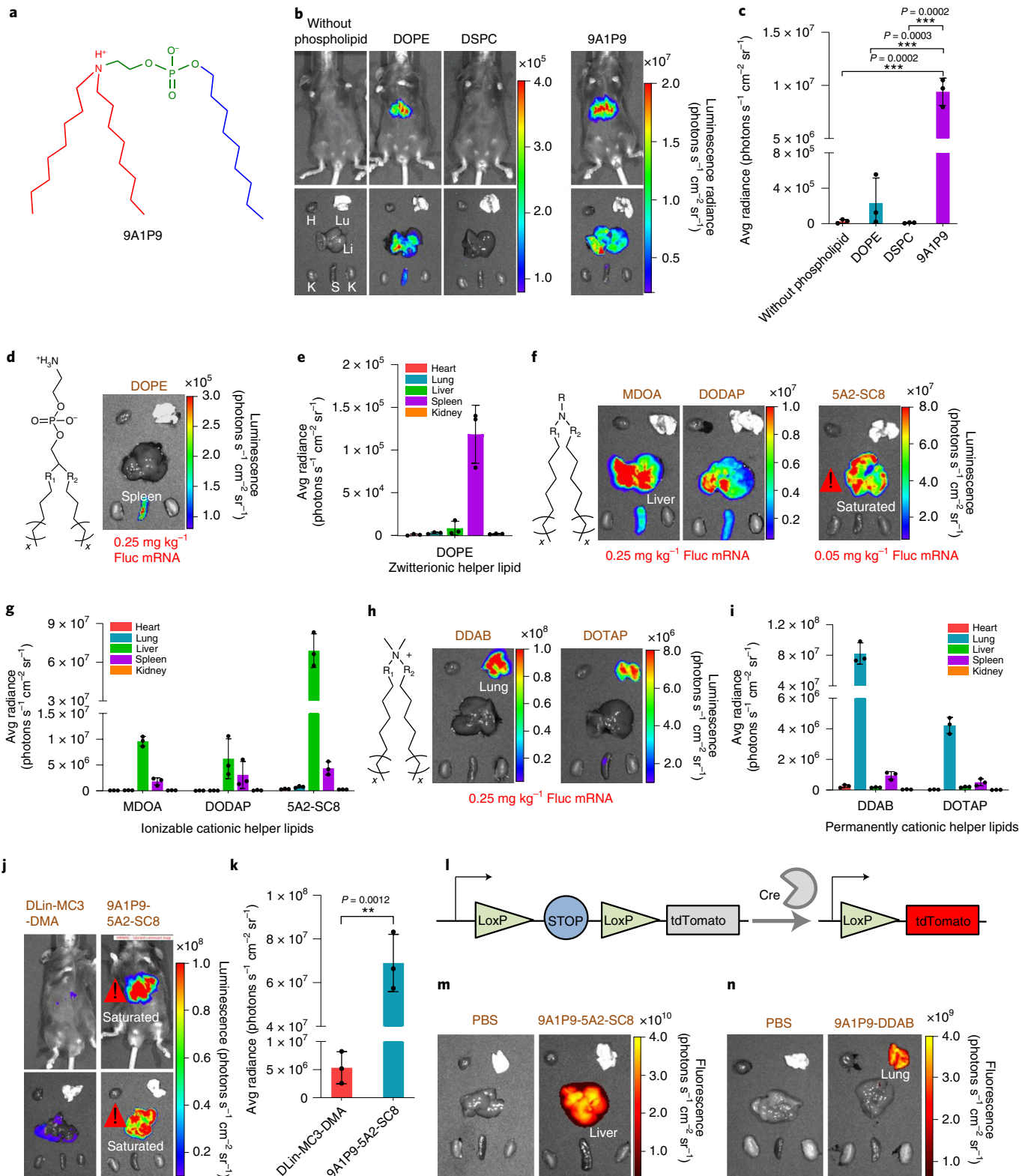
To verify the ability of iPLNPs to induce organ-selective gene editing, we used an activatable Cre-LoxP mouse model that expresses Lox-stop-Lox tdTomato in all tissues. Through iPLNP delivery of Cre-recombinase mRNA (Cre mRNA), the translated Cre protein can delete the stop cassette and turn on red tdTomato fluorescence only in successfully transfected cells (Fig. 5l). Highly efficient and organ-selective gene editing was observed 2 days following Cre mRNA delivery (Fig. 5m,n). We next used this model to quantify transfection of specific cell types in liver, lung and spleen organs. Following delivery of Cre mRNA, liver-selective 9A1P9-5A2-SC8 iPLNPs mediated mRNA delivery to roughly 91% of all hepatocytes (Supplementary Fig. 24). Lung-selective 9A1P9-DDAB iPLNPs transfected roughly 34% of all endothelial cells, roughly 20% of all epithelial cells and roughly 13% of immune cells (Supplementary Fig. 25). Spleen-selective 10A1P16-MDOA iPLNPs transfected roughly 30% of all macrophages and 6% of all B cells (Supplementary Fig. 26). These results demonstrate the potential of organ-selective iPLNPs for diverse therapeutic applications. iPLNP proposed here represents one of the most efficacious mRNA delivery systems and holds great potential for organ-selective CRISPR-Cas9 gene editing.

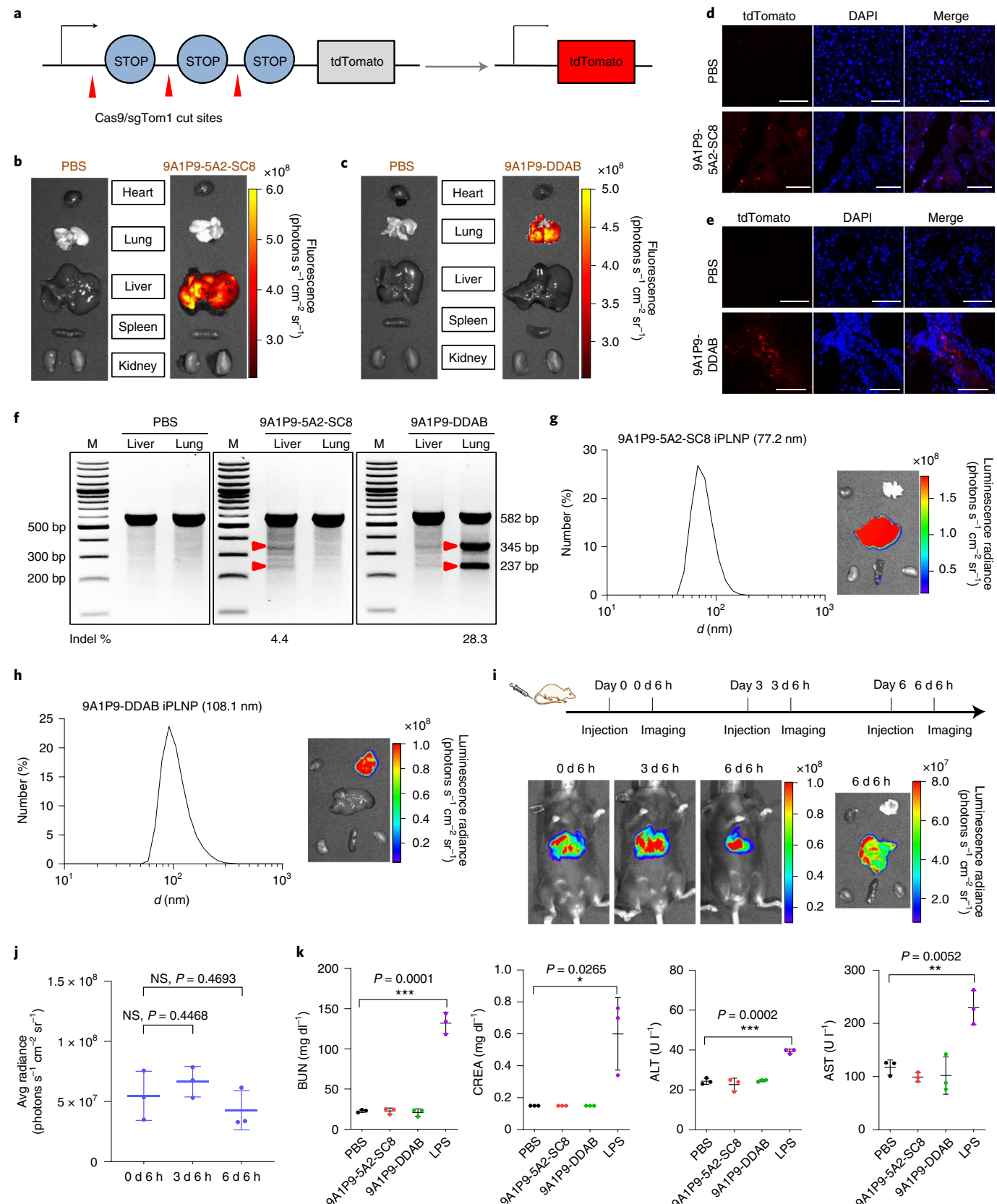
Organ-specific CRISPR-Cas editing with translation potential. Although LNPs have been used to deliver mRNA, there are still few reports for successful in vivo Cas9 mRNA/sgRNA delivery for CRISPR-Cas gene editing^{8,9} and even less so with precision to specific organs²⁷. We next used iPLNPs to codeliver Cas9 mRNA and sgRNA for gene editing. 9A1P9-5A2-SC8 and 9A1P9-DDAB iPLNPs containing Cas9 mRNA and Tom1 sgRNA (sgTom1) with a 4:1 weight ratio were intravenously (i.v.) administered into A19 mice at a total RNA dose of 0.75 mg kg^{-1} , which would delete the stop cassettes and activate tdTomato protein (Fig. 6a). Fluorescent tdTomato protein was observed specifically in the liver after 9A1P9-5A2-SC8 iPLNP administration by ex vivo organ imaging (Fig. 6b). Sectioned organ analysis by confocal fluorescence microscopy showed tdTomato-positive cells in liver tissues (Fig. 6d). Similarly, 9A1P9-DDAB iPLNP induced specific gene editing in the lungs (Fig. 6c,e). Following this, phosphatase and tensin homologue sgRNA (sgPTEN) was codelivered with Cas9 mRNA for gene editing in C57BL/6 mice (Cas9 mRNA/sgPTEN weight ratio, 4:1; total RNA dose, 0.75 mg kg^{-1}) targeting an endogenous gene. T7E1 assay showed efficient target gene editing in liver and lung by 9A1P9-5A2-SC8 and 9A1P9-DDAB iPLNPs, respectively (Fig. 6f and Supplementary Fig. 27). CRISPR-Cas9 gene editing in specific organs has remained a long-standing challenge and the highly efficient and organ-selective gene editing might broaden the iPLNP application to diverse genetic diseases.

Fig. 5 | iPhos outperformed traditional phospholipids, and functioned with different helper lipids for organ-selective RNA delivery. **a**, Structure of iPhos 9A1P9 in the acidic endosomal environment. **b,c**, iPhos 9A1P9 outperformed benchmark DOPE and DSPC for mRNA delivery. Images (**b**) and quantification (**c**) of luciferase expression in liver were recorded (Fluc mRNA, 0.25 mg kg^{-1}). H, heart; Lu, lung; Li, liver; K, kidney; S, spleen. **d,e**, iPLNPs containing zwitterionic helper lipid DOPE mediated mRNA expression in spleen. In vivo evaluation (**d**) and quantification (**e**) were evaluated (Fluc mRNA, 0.25 mg kg^{-1}). **f,g**, iPLNPs containing ionizable cationic helper lipids mediated mRNA translation in liver. Organ selectivity (**f**) and quantification (**g**) of Fluc mRNA expression by 9A1P9 iPLNP with different ionizable cationic helper lipids were assayed (Fluc mRNA, 0.25 mg kg^{-1} for MDOA and DODAP; 0.05 mg kg^{-1} for 5A2-SC8). **h,i**, iPLNPs containing permanently cationic helper lipids induced mRNA transfection in lung. Organ images (**h**) and quantification (**i**) of Fluc mRNA expression by 9A1P9 iPLNP using DDAB and DOTAP were evaluated (Fluc mRNA, 0.25 mg kg^{-1}). **j,k**, 9A1P9-5A2-SC8 iPLNP showed much higher mRNA delivery efficacy than positive control DLin-MC3-DMA LNPs. Images (**j**) and quantification (**k**) of luciferase expression in liver were recorded (Fluc mRNA, 0.05 mg kg^{-1}). **l–n**, 9A1P9 iPLNPs enabled Cre mRNA delivery selectively in liver or lung. Schematic (**l**) represented a Cre-LoxP mouse model that could express tdTomato by translating Cre-recombinase mRNA to Cre protein to delete the stop. 9A1P9-5A2-SC8 iPLNP (**m**) and 9A1P9-DDAB iPLNP (**n**) mediated tdTomato expression in liver and lung, respectively (Cre mRNA, 0.25 mg kg^{-1}). All data are presented as mean \pm s.d. ($n=3$ biologically independent mice). Statistical significance was analysed by the two-tailed unpaired t-test: *** $P < 0.0001$; ** $P < 0.001$; * $P < 0.01$; $^{\circ}P < 0.05$.

Considering potential preclinical activities, lead iPLNPs were manufactured at higher scale using controlled microfluidic mixing. Precise control over the mixing speed and volume ratios enabled the preparation of smaller 9A1P9-5A2-SC8 iPLNPs (77.2 nm, liver-specific), 9A1P9-DDAB iPLNPs (108.1 nm, lung-specific) and 10A1P16-MDOA iPLNPs (96.1 nm, spleen-specific). High *in vivo* mRNA delivery efficiency and precise organ selectivity were fully retained after decreasing

iPLNP diameters (Fig. 6g,h and Supplementary Fig. 28). Furthermore, iPLNPs allowed repeat dosing, where high efficacy was retained after each repeat injection (Fig. 6i,j and Supplementary Fig. 29). Analysis of liver function enzymes and tissue section histology indicated that these iPLNPs showed negligible *in vivo* toxicity at the tested doses (Fig. 6k and Supplementary Figs. 30 and 31). These results highlight the potential of iPLNP system for future applications.





Discussion

The CRISPR-Cas9 gene editing system is gaining increasing interest due to its tremendous potential for genetic disease treatment^{4,52,53}. Although cells build membranes and mediate transport

using phospholipids, almost all efficacious LNPs for gene delivery rely on ionizable amines as the key physicochemical parameter to mediate endosomal escape via charge acquisition^{11–13}. In carrier development, synthetic zwitterionic lipids are largely unexplored,

Fig. 6 | iPLNPs enabled CRISPR-Cas9 gene editing selectively in liver and lungs and possessed potential for clinical translation. **a**, Schematic of codelivery of Cas9 mRNA and sgTom1 deletes the stop cassettes and activates tdTomato protein. **b**, 9A1P9-5A2-SC8 iPLNPs enabled gene editing specifically in liver. **c**, 9A1P9-DDAB iPLNPs enabled gene editing specifically in lung. **d**, Following i.v. administration of 9A1P9-5A2-SC8 iPLNPs containing Cas9 mRNA and sgTom1 to Ai9 mice, tdTomato-positive cells were observed in liver. Scale bars, 50 μm. **e**, Confocal fluorescence images showed tdTomato-positive cells in lung after administration of 9A1P9-DDAB iPLNPs. Scale bars, 50 μm. **f**, T7E1 assay of organ-selective gene editing. 9A1P9-5A2-SC8 and 9A1P9-DDAB iPLNPs containing Cas9 mRNA and sgPTEN were i.v. administered into C57BL/6 mice, enabling CRISPR-Cas9 gene editing in liver and lung, respectively. For all the CRISPR-Cas9 gene editing assays, Cas9 mRNA/sgrNA weight ratio of 4:1 and total RNA dose of 0.75 mg kg⁻¹ were used. **g,h**, iPLNPs were prepared by controlled microfluidic mixing, which resulted in decreased iPLNP sizes and preserved efficacy and organ selectivity. 9A1P9-5A2-SC8 iPLNPs (liver-specific, Fluc mRNA, 0.05 mg kg⁻¹) (**g**) and 9A1P9-DDAB iPLNPs (lung-specific, Fluc mRNA, 0.25 mg kg⁻¹) (**h**) demonstrated small sizes and fully retained precise organ selectivity. **i,j**, 9A1P9-5A2-SC8 iPLNPs (Fluc mRNA, 0.05 mg kg⁻¹) allowed repeat dosing without loss of efficacy. Whole body imaging (**i**) and quantification of luciferase expression (**j**) was performed 6 h after each injection. **k**, 9A1P9-5A2-SC8 and 9A1P9-DDAB iPLNPs were well tolerated in vivo. Data are presented as mean ± s.d. and statistical significance was analysed by the two-tailed unpaired t-test: ***P < 0.0001; **P < 0.001; *P < 0.05; NS, P > 0.05. All data are from n = 3 biologically independent mice.

even though they may readily enable endosomal membrane fusion and leakiness due to their similarity to biological membranes.

We were therefore inspired to design and synthesize iPhos lipids to overcome these challenges. Optimized iPhos lipids include a pH-switchable small zwitterion head and a three-tail body. This unique architecture makes it easy to insert into naturally occurring membrane phospholipids and induce phase transformation for increased RNA release from endosomes. SAR revealed that iPhos chain lengths can control in vivo mRNA delivery efficacy and organ selectivity. Moreover, diverse existing zwitterionic, ionizable cationic and permanently cationic helper lipids were evaluated in our iPLNP system, which mediated mRNA translation selectively in spleen, liver and lungs. Ultimately, the top 9A1P9-5A2-SC8 and 9A1P9-DDAB iPLNPs were used to codeliver mRNA and sgrNA to edit reporter and endogenous genes, and long-term challenging organ-selective CRISPR-Cas9 gene editing was achieved. Additionally, these iPLNPs showed broad applicability to deliver other nucleic acids, including plasmid DNA and siRNA (Supplementary Fig. 32). These profiles impart synthetic ionizable phospholipids great promise for the treatment of diverse genetic diseases with minimized side effects.

Online content

Any methods, additional references, Nature Research reporting summaries, source data, extended data, supplementary information, acknowledgements, peer review information; details of author contributions and competing interests; and statements of data and code availability are available at <https://doi.org/10.1038/s41563-020-00886-0>.

Received: 25 March 2020; Accepted: 20 November 2020;

Published online: 4 February 2021

References

- Wang, H. X. et al. CRISPR/Cas9-based genome editing for disease modeling and therapy: challenges and opportunities for nonviral delivery. *Chem. Rev.* **117**, 9874–9906 (2017).
- Hajj, K. A. & Whitehead, K. A. Tools for translation: non-viral materials for therapeutic mRNA delivery. *Nat. Rev. Mater.* **2**, 17056 (2017).
- Jinek, M. et al. A programmable dual-RNA-guided DNA endonuclease in adaptive bacterial immunity. *Science* **337**, 816–821 (2012).
- Cong, L. et al. Multiplex genome engineering using CRISPR/Cas systems. *Science* **339**, 819–823 (2013).
- Mali, P. et al. RNA-guided human genome engineering via Cas9. *Science* **339**, 823–826 (2013).
- Shahbazi, R. et al. Targeted homology-directed repair in blood stem and progenitor cells with CRISPR nanoformulations. *Nat. Mater.* **18**, 1124–1132 (2019).
- Yin, H. et al. Structure-guided chemical modification of guide RNA enables potent non-viral in vivo genome editing. *Nat. Biotechnol.* **35**, 1179 (2017).
- Miller, J. B. et al. Non-viral CRISPR/Cas gene editing in vitro and in vivo enabled by synthetic nanoparticle co-delivery of Cas9 mRNA and sgrNA. *Angew. Chem. Int. Ed.* **56**, 1059–1063 (2017).
- Liu, J. et al. Fast and efficient CRISPR/Cas9 genome editing in vivo enabled by bioreducible lipid and messenger RNA nanoparticles. *Adv. Mater.* **31**, 1902575 (2019).
- Kanasty, R., Dorkin, J. R., Vegas, A. & Anderson, D. Delivery materials for siRNA therapeutics. *Nat. Mater.* **12**, 967–977 (2013).
- Semple, S. C. et al. Rational design of cationic lipids for siRNA delivery. *Nat. Biotechnol.* **28**, 172–176 (2010).
- Jayaraman, M. et al. Maximizing the potency of siRNA lipid nanoparticles for hepatic gene silencing in vivo. *Angew. Chem. Int. Ed.* **51**, 8529–8533 (2012).
- Love, K. et al. Lipid-like materials for low-dose, in vivo gene silencing. *Proc. Natl Acad. Sci. USA* **107**, 1864–1869 (2010).
- Cheng, Q. et al. Dendrimer-based lipid nanoparticles deliver therapeutic FAH mRNA to normalize liver function and extend survival in a mouse model of hepatorenal tyrosinemia type I. *Adv. Mater.* **30**, e1805308 (2018).
- Sabnis, S. et al. A novel amino lipid series for mRNA delivery: improved endosomal escape and sustained pharmacology and safety in non-human primates. *Mol. Ther.* **26**, 1509–1519 (2018).
- van Meer, G., Voelker, D. R. & Feigenson, G. W. Membrane lipids: where they are and how they behave. *Nat. Rev. Mol. Cell Biol.* **9**, 112–124 (2008).
- Miller, J. B., Kos, P., Tieu, V., Zhou, K. & Siegwart, D. J. Development of cationic quaternary ammonium sulfonamide amino lipids for nucleic acid delivery. *ACS Appl. Mater. Inter.* **10**, 2302–2311 (2018).
- Gilleron, J. et al. Image-based analysis of lipid nanoparticle-mediated siRNA delivery, intracellular trafficking and endosomal escape. *Nat. Biotechnol.* **31**, 638–646 (2013).
- Wittrup, A. et al. Visualizing lipid-formulated siRNA release from endosomes and target gene knockdown. *Nat. Biotechnol.* **33**, 870–876 (2015).
- Miller, J. B. & Siegwart, D. J. Design of synthetic materials for intracellular delivery of RNAs: from siRNA-mediated gene silencing to CRISPR/Cas gene editing. *Nano Res.* **11**, 5310–5337 (2018).
- Whitehead, K. A. et al. Degradable lipid nanoparticles with predictable in vivo siRNA delivery activity. *Nat. Commun.* **5**, 4277 (2014).
- Miao, L. et al. Delivery of mRNA vaccines with heterocyclic lipids increases anti-tumor efficacy by STING-mediated immune cell activation. *Nat. Biotechnol.* **37**, 1174–1185 (2019).
- Kaczmarek, J. C. et al. Optimization of a degradable polymer-lipid nanoparticle for potent systemic delivery of mRNA to the lung endothelium and immune cells. *Nano Lett.* **18**, 6449–6454 (2018).
- Paunovska, K. et al. Nanoparticles containing oxidized cholesterol deliver mRNA to the liver microenvironment at clinically relevant doses. *Adv. Mater.* **31**, 1807748 (2019).
- Fenton, O. S. et al. Bioinspired alkenyl amino alcohol ionizable lipid materials for highly potent in vivo mRNA delivery. *Adv. Mater.* **28**, 2939–2943 (2016).
- Truong, B. et al. Lipid nanoparticle-targeted mRNA therapy as a treatment for the inherited metabolic liver disorder arginase deficiency. *Proc. Natl Acad. Sci. USA* **116**, 21150–21159 (2019).
- Cheng, Q. et al. Selective organ targeting (SORT) nanoparticles for tissue specific mRNA delivery and CRISPR/Cas gene editing. *Nat. Nanotechnol.* **15**, 313–320 (2020).
- Hajj, K. A. et al. Branched-tail lipid nanoparticles potently deliver mRNA In vivo due to enhanced ionization at endosomal pH. *Small* **15**, 1805097 (2019).
- Fenton, O. S. et al. Synthesis and biological evaluation of ionizable lipid materials for the in vivo delivery of messenger RNA to B lymphocytes. *Adv. Mater.* **29**, 1606944 (2017).
- Alabi, C. A. et al. Multiparametric approach for the evaluation of lipid nanoparticles for siRNA delivery. *Proc. Natl Acad. Sci. USA* **110**, 12881–12886 (2013).
- Hou, X. et al. Vitamin lipid nanoparticles enable adoptive macrophage transfer for the treatment of multidrug-resistant bacterial sepsis. *Nat. Nanotechnol.* **15**, 41–46 (2020).

32. Menger, F. M. & Peresypkin, A. V. A combinatorially-derived structural phase diagram for 42 zwitterionic geminis. *J. Am. Chem. Soc.* **123**, 5614–5615 (2001).
33. Wang, D. et al. Supramolecularly engineered phospholipids constructed by nucleobase molecular recognition: upgraded generation of phospholipids for drug delivery. *Chem. Sci.* **6**, 3775–3787 (2015).
34. Akinc, A. et al. A combinatorial library of lipid-like materials for delivery of RNAi therapeutics. *Nat. Biotechnol.* **26**, 561–569 (2008).
35. Zhou, K. et al. Modular degradable dendrimers enable small RNAs to extend survival in an aggressive liver cancer model. *Proc. Natl Acad. Sci. USA* **113**, 520–525 (2016).
36. Liu, S. et al. Highly branched poly(β-amino ester) delivery of minicircle DNA for transfection of neurodegenerative disease related cells. *Nat. Commun.* **10**, 3307 (2019).
37. Zhou, J. et al. Biodegradable poly(amine-co-ester) terpolymers for targeted gene delivery. *Nat. Mater.* **11**, 82–90 (2012).
38. Liu, S. et al. Bioreducible zinc(II)-coordinative polyethylenimine with low molecular weight for robust gene delivery of primary and stem cells. *J. Am. Chem. Soc.* **139**, 5102–5109 (2017).
39. Dahlman, J. E. et al. In vivo endothelial siRNA delivery using polymeric nanoparticles with low molecular weight. *Nat. Nanotechnol.* **9**, 648–655 (2014).
40. Schlame, M. et al. The physical state of lipid substrates provides transacylation specificity for tafazzin. *Nat. Chem. Bio.* **8**, 862–869 (2012).
41. Hafez, I. M., Maurer, N. & Cullis, P. R. On the mechanism whereby cationic lipids promote intracellular delivery of polynucleic acids. *Gene Ther.* **8**, 1188–1196 (2001).
42. Wei, T. et al. Anticancer drug nanomicelles formed by self-assembling amphiphilic dendrimer to combat cancer drug resistance. *Proc. Natl Acad. Sci. USA* **112**, 2978–2983 (2015).
43. Walsh, C. L., Nguyen, J. & Szoka, F. C. Synthesis and characterization of novel zwitterionic lipids with pH-responsive biophysical properties. *Chem. Commun.* **48**, 5575–5577 (2012).
44. Zhang, Y. et al. The development of an in vitro assay to screen lipid based nanoparticles for siRNA delivery. *J. Controlled Release* **174**, 7–14 (2014).
45. Cheng, Y., Yumul, R. C. & Pun, S. H. Virus-inspired polymer for efficient in vitro and in vivo gene delivery. *Angew. Chem. Int. Ed.* **55**, 12013–12017 (2016).
46. Zhou, D. et al. The transition from linear to highly branched poly(beta-amino ester)s: branching matters for gene delivery. *Sci. Adv.* **2**, e1600102 (2016).
47. Kowalski, P. S. et al. Ionizable amino-polyesters synthesized via ring opening polymerization of tertiary amino-alcohols for tissue selective mRNA delivery. *Adv. Mater.* **30**, 1801151 (2018).
48. Li, B. et al. An orthogonal array optimization of lipid-like nanoparticles for mRNA delivery in vivo. *Nano Lett.* **15**, 8099–8107 (2015).
49. Wei, T., Cheng, Q., Min, Y. L., Olson, E. N. & Siegwart, D. J. Systemic nanoparticle delivery of CRISPR-Cas9 ribonucleoproteins for effective tissue specific genome editing. *Nat. Commun.* **11**, 3232 (2020).
50. Akinc, A. et al. The Onpattro story and the clinical translation of nanomedicines containing nucleic acid-based drugs. *Nat. Nanotechnol.* **14**, 1084–1087 (2019).
51. Patel, S. et al. Naturally-occurring cholesterol analogues in lipid nanoparticles induce polymorphic shape and enhance intracellular delivery of mRNA. *Nat. Commun.* **11**, 983 (2020).
52. Xue, W. et al. CRISPR-mediated direct mutation of cancer genes in the mouse liver. *Nature* **514**, 380–384 (2014).
53. Staahl, B. T. et al. Efficient genome editing in the mouse brain by local delivery of engineered Cas9 ribonucleoprotein complexes. *Nat. Biotechnol.* **35**, 431–434 (2017).

Publisher's note Springer Nature remains neutral with regard to jurisdictional claims in published maps and institutional affiliations.

© The Author(s), under exclusive licence to Springer Nature Limited 2021

Methods

Materials. COP and triethylamine were purchased from Fisher Scientific. Amines, alcohols, cholesterol and MDOA were purchased from Sigma-Aldrich. DOPE, 1,2-dioleoyl-sn-glycero-3-phospho-L-serine (sodium salt) (DOPS), 1,2-dioleoyl-sn-glycero-3-phosphocholine (DOPC), 1,2-dioleoyl-sn-glycero-3-phosphoethanolamine-N-(7-nitro-2,1,3-benzoxadiazol-4-yl) (ammonium salt) (NBD-PE), 1,2-dioleoyl-sn-glycero-3-phosphoethanolamine-N-(lissamine rhodamine B sulfonyl) (ammonium salt) (Rho-PE), DSPC, DODAP, DOTAP (chloride salt) and dimethyldioctadecylammonium (bromide salt) (DDAB) were purchased from Avanti Lipids. 1,2-dimyristoyl-rac-glycero-3-methoxy(poly(ethylene glycol))-2000 (DMG-PEG2000) was obtained from NOF America. DLin-MC3-DMA was purchased from MedKoo Biosciences, and its LNP was prepared at the molar ratio of 50:10:38.5:1.5 (DLin-MC3-DMA:DSPC:cholesterol:DMG-PEG2000). Dulbecco's modified phosphate buffered saline (PBS), RPMI-1640 medium, fetal bovine serum and trypsin-EDTA (0.25%) were purchased from Sigma-Aldrich. Firefly luciferase mRNA, Cre mRNA and Cas9 mRNA were purchased from TriLink Biotechnologies. The Quant-iT RiboGreen RNA assay kit was purchased from Life Technologies. ONE-Glo + Tox luciferase assay kit was purchased from Promega. D-Luciferin firefly, sodium salt monohydrate was purchased from Gold Biotechnology.

Synthesis of alkylated dioxaphospholane oxide molecules P4–P16. P4–P16 were synthesized via esterification of COP by corresponding alcohols with different alkyl chain length. For instance, to prepare P4, 1-butanol (30 mmol) and triethylamine (30 mmol) were dissolved in 25 ml of anhydrous tetrahydrofuran. Then COP (30 mmol) solution in 10 ml of tetrahydrofuran was added dropwise to the mixture at -15°C . Afterwards, the reaction continued at 25°C for 12 h. The mixture was filtered to remove the triethylamine hydrochloride and the filtrate was concentrated by rotary evaporation to give P4. P5–P10 molecules were synthesized using respective alcohols and following the general protocol described above. For P11–P16 synthesis, COP was added to corresponding alcohols at 0°C and other procedures were retained the same. All P4–P16 synthesis gave the yields over 90%.

General synthesis of ionizable phospholipids (iPhos) library. iPhos ($n\text{AxPm}$) were synthesized through orthogonal reactions by amines (1A–28A) and alkylated dioxaphospholane oxide molecules (Pm , $m = 4–16$). ‘ x ’ indicates the Pm molecule number modified on one amine molecule, and each Pm molecule could introduce one phosphate group and one hydrophobic alkyl chain into the iPhos. Each primary, secondary, or tertiary amine was designed to consume one equivalent of alkylated dioxaphospholane oxide molecules Pm . For amines nA ($n = 1–18$) with a single primary, secondary or tertiary amine, 1.1 equivalents of Pm were reacted with amines to obtain nA1Pm. For nA ($n = 19–28$) with multiple amine groups, each amine group was designed to introduce one zwitterion at the most. Briefly, the amines were reacted with 2.2, 3.3, 4.4 and 5.5 equivalents of Pm to give nA2Pm, nA3Pm, nA4Pm and nA5Pm iPhos, respectively. All the reactions were conducted in anhydrous dimethyl sulfoxide (DMSO) at the starting material concentration of 0.3 g ml^{-1} . The mixtures were stirred at 70°C for 3 d, then DMSO was removed through vacuum drying.

Initial mRNA delivery (in vitro and in vivo screening) experiments were conducted using crude iPhos. Selected top iPhos (for example, 9A1P9, 10A1P10, 9A1P15 and 10A1P16) were purified by column flash chromatography and used for additional characterizations (including size, zeta potential, mRNA binding, pK_a , haemolysis, FRET studies and so on) and in vivo evaluations. The products were eluted and fractionated in silica gel column with a solvent gradient of 3% chloroform in methanol to 10% chloroform in methanol. The final iPhos were concentrated by rotary evaporation and dried under vacuum for 24 h.

In vitro iPhos nanoparticle (iPLNP) formulation and characterization. iPLNPs were prepared by the ethanol dilution method. mRNA was diluted in citric acid/sodium citrate buffer (10 mM, pH 4.4). The lipid mixture containing synthetic iPhos, MDOA, cholesterol and DMG-PEG2000 was prepared in ethanol. The two solutions were rapidly mixed by pipette at a 3:1 aqueous:ethanol volumetric ratio. Post incubation for 15 min, the nanoparticles were diluted threefold with 1× PBS buffer for in vitro mRNA delivery.

For particle size and Ribogreen mRNA binding measurement, the nanoparticles were diluted fivefold with 1× PBS buffer. Zeta potential was recorded with nanoparticles diluted by tenfold with 1× PBS buffer. Zetasizer Nano ZS (Malvern, v.7.13) with a He-Ne laser ($\lambda = 632\text{ nm}$) was used for particle size and zeta potential measurement. For transmission electron microscopy (TEM) assay, mRNA-loaded iPLNPs were prepared and dialysed against H_2O in Pur-A-Lyzer midi dialysis chambers (Sigma-Aldrich) for 1 h (total lipid concentration, 2 mg ml^{-1}). Then 5–8 μl of iPLNP solutions were dropped onto carbon TEM grids, allowing to deposit for 1 min before blotting with filter paper, then the TEM grids were imaged (FEI Tecnai G2 Spirit Biotwin).

Phase transformation assay by ^{31}P NMR spectra. Endosomal membrane mimicking liposomes were prepared by mixing DOPS:DOPC:DOPE (molar ratio 25:25:50) in chloroform, followed by rotary evaporation and overnight vacuum dry to give a thin lipid film. The films were hydrated in D_2O (20 mM

4-(2-hydroxyethyl)-1-piperazineethanesulfonic acid (HEPES), pH 5.5), and the solution was vortex mixed vigorously to get a white dispersion. The dispersion was further hydrated by maintaining overnight at room temperature and then was underwent five freeze–thaw cycles with liquid nitrogen. ^{31}P NMR spectrum of endosomal mimics was recorded. Afterward, iPhos lipid 9A1P9 was dissolved in chloroform, rotary evaporated and vacuum dried overnight to give a thin lipid film. Then, D_2O (20 mM HEPES, pH 5.5) was added and sonicated to get the white suspended dispersion. Above endosomal mimics and 9A1P9 suspension were mixed thoroughly by sonication (9A1P9:DOPS:DOPC:DOPE molar ratio, 20:20:20:40), and the dispersion became much clearer. The solution underwent five more freeze–thaw cycles with liquid nitrogen, and the solution became white dispersion again, which was characterized by ^{31}P NMR. A total of 10 μmol of lipids was used. ^{31}P NMR spectra were performed on a Bruker 400 MHz spectrometer at 25°C . Acquisition parameters included 0.68 s acquisition time, 1 s relaxation delay and 7,500 scans.

Haemolysis assay. Mouse red blood cells (RBCs) were isolated from freshly collected whole blood by centrifuging at 10,000g for 5 min, then the RBCs were washed five times with PBS buffer (pH 7.4). Afterwards, RBCs were suspended in PBS of pH 7.4 and 5.5, respectively. iPLNPs were formulated using the in vitro iPLNP formulation method outlined above. Lipids were dissolved in chloroform, rotary evaporated and vacuum dried for another 2 h to give a thin lipid film. Then, PBS (pH 7.4) was added and sonicated for 20 min to obtain particle suspension. RBC suspension was added to 96-well plates, and calculated iPLNPs or lipids were added to the wells. After incubating at 37°C for 1 h, the RBC solutions were centrifuged at 10,000g for 5 min and the supernatants containing haemoglobin were collected. The haemoglobin contents were evaluated at a wavelength of 540 nm with a microplate reader. That RBC suspension incubated in PBS was set as negative control, and RBC suspension incubated in Triton X-100 solutions (1 wt.%) was set as positive control. Cell viability of iPhos lipids and iPLNPs with same conditions was measured, confirming that haemolysis was not due to cytotoxicity.

Lipid fusion by FRET assay. Lipid mixing and fusion with endosomal mimicking anionic liposomes were determined by a FRET assay. The DOPE-conjugated FRET probes NBD-PE and Rho-PE were formulated into the same endosomal mimicking nanoparticle, leading to attenuated NBD fluorescence because of FRET to rhodamine. Once lipid fusion occurred, NBD signal would increase due to the larger distance between the two probes. Endosomal mimicking anionic liposomes were prepared by mixing DOPS:DOPC:DOPE:NBD-PE:Rho-PE (molar ratio 25:25:48:1:1) in chloroform, followed by rotary evaporation and another 2 h vacuum dry to give a thin lipid film. The dried film was subsequently hydrated in PBS (pH 7.4), sonicated for 20 min and total lipid concentration was fixed at 1 mM. iPLNPs were formulated using the in vitro iPLNP formulation method outlined above with an iPhos concentration of 1 mM. iPhos 10A1P10 was dissolved in chloroform, and rotary evaporated to give a thin lipid film. Then, PBS (pH 7.4) was added and sonicated for 20 min to obtain particle suspension (10 mM). 25A3P10 with multiple zwitterions failed to form particle suspension after sonication, so only lipid fusion of 25A3P10 iPLNPs was evaluated. PBS (pH 5.5) was added to black 96-well plates (1001 per well), and 1 μl of endosomal mimicking anionic liposomes (1 mM) was added to each well. Then 10 μl of iPLNPs or 1 μl of lipid suspensions were added to the wells. After incubating at 37°C for 5 min, fluorescence measurements (F) were conducted on a microplate reader at $\text{Ex}/\text{Em} = 465/520\text{ nm}$. Only endosomal mimicking anionic liposomes in PBS were set as negative control (F_{\min}). Lipids containing probes incubated with Triton X-100 solutions (2 wt.%) were set as positive control (F_{\max}). The lipid fusion (%) was calculated as $(F - F_{\min})/(F_{\max} - F_{\min}) \times 100\%$.

In vitro screening of iPhos for mRNA delivery. IGROV1 cells were seeded at a density of 1×10^4 cells per well in white opaque 96-well plates. Then, 24 h later, nanoparticles with Fluc mRNA were prepared using the in vitro iPLNP formulation method outlined above in 96-well plates by rapid mixing of aqueous phase and ethanol phase ($v/v = 3:1$) with a multichannel pipette. iPLNPs were prepared at synthetic iPhos:mRNA molar ratio of 11,622:1 and lipid mixture synthetic iPhos:MDOA:cholesterol:DMG-PEG2000 molar ratio of 25:30:30:1. The synthetic iPhos:mRNA molar ratio of 11622:1 was fixed, where 10A1P4–12A1P16: mRNA showed an average weight ratio of 10 ± 2.5 . This could ensure that each iPLNP had same moles of lipid mixture. The ratios were also used for other characterizations and in vivo evaluation, unless otherwise noted. Per well, 50 ng of mRNA was used. Then, 150 μl of fresh cell culture media were used to replace the previous media, and the formulated iPLNPs were added into the cells. After another 24 h incubation, luciferase expression and cell viability were evaluated with the ONE-Glo + Tox luciferase assay kits.

In vivo iPLNP formulation and characterization. The mRNA was diluted in citric acid/sodium citrate buffer (10 mM, pH 3.2). The lipid mixture containing synthetic iPhos, MDOA (or other help lipids), cholesterol and DMG-PEG2000 was prepared in ethanol. The two phases were rapidly mixed by pipette at a 3:1 aqueous:ethanol volumetric ratio. Post incubation for 15 min, iPLNPs were dialysed against 1× PBS in Pur-A-Lyzer midi dialysis chambers (Sigma-Aldrich) for in vivo use. Unless otherwise noted, iPLNPs were formulated by pipette.

To further decrease the sizes, iPLNPs were prepared using the NanoAssemblr microfluidic mixing system (Precision Nanosystems). Same as above, mRNA was diluted in citric acid/sodium citrate buffer (10 mM, pH 3.2), and lipid mixtures were dissolved in ethanol. The two phases were rapidly mixed at a 3:1 aqueous:ethanol volumetric ratio with a flow rate of 9 ml min⁻¹. A waste collection of 0.3 ml at the start and 0.1 ml in the end was set. Post incubation for 15 min, iPLNPs were dialysed against 1× PBS for future use.

In vivo luciferase mRNA delivery. For iPhos in vivo screening, nanoparticles containing Fluc mRNA were prepared as in vivo iPLNP formulation method mentioned above. Unless otherwise noted, the ratios of formulations were in accordance with that of the in vitro screening. Briefly, iPLNPs were prepared at synthetic iPhos:Fluc mRNA molar ratio of 11,622:1 and lipid mixture synthetic iPhos:MDOA:cholesterol:DMG-PEG2000 molar ratio of 25:30:30:1. Then, the nanoparticles were administered to female C57BL/6 mice (6–8 weeks old) via i.v. injection. 6 h later, the luciferase expression was evaluated by live animal bioluminescence imaging. Briefly, mice were anaesthetized under isoflurane and 100 µl of d-luciferin (GoldBio, 30 mg ml⁻¹ in PBS) substrate was intraperitoneally injected. After 5 min under anaesthesia, the luciferase activity was imaged on an IVIS Lumina system (Perkin Elmer). Afterwards, the organs were isolated and imaged with the same method. The images were processed with the Living Image software v.4.3 (64-bit, Caliper Life Sciences).

iPhos 9A1P9 was used to compare with commercial phospholipids DOPE and DSPC. C57BL/6 mice were i.v. injected with nanoparticles at 0.25 mg kg⁻¹ of Fluc mRNA and luminescence was quantified 6 h post injection. 9A1P9:MDOA:cholesterol:DMG-PEG2000 molar ratio of 25:30:30:1 and 9A1P9:mRNA weight ratio of 18:1 were used. For commercial phospholipid comparison, equimolar DOPE or DSPC were used to replace 9A1P9. Other procedures were conducted the same as mentioned above.

For 9A1P9 iPLNPs with different helper lipids, 9A1P9:DOPE:cholesterol:DMG-PEG2000 (molar ratio) of 55:30:45:0.2, 9A1P9:MDOA (DODAP or 5A2-SC8):cholesterol:DMG-PEG2000 (molar ratio) of 25:30:30:1 and 9A1P9:DDAB (or DOTAP):cholesterol:DMG-PEG2000 (molar ratio) of 60:30:40:0.4 were used. For all the formulations, 9A1P9:mRNA weight ratio was fixed at 18:1. Bioluminescence imaging was conducted at different time intervals (3, 6, 12 and 24 h), following i.v. injection of various Fluc mRNA doses (0.05 to 0.25 mg kg⁻¹). Other procedures were conducted the same as mentioned above.

In vivo codelivery of Cas9 mRNA and sgTom1 for gene editing.

Nanoparticles containing Cas9 mRNA and modified sgTom1 (mRNA:sgRNA weight ratio 4:1, total RNA dose 0.75 mg kg⁻¹) were prepared as in vivo iPLNP formulation method mentioned above (Supplementary Table 2). 9A1P9:5A2-SC8:cholesterol:DMG-PEG2000 (molar ratio) of 25:30:30:1 and 9A1P9:DDAB:cholesterol:DMG-PEG2000 (molar ratio) of 60:30:40:0.4 were used for 9A1P9-5A2-SC8 iPLNP and 9A1P9-DDAB iPLNP, respectively. The 9A1P9 to RNA weight ratio was fixed at 18 to 1. Afterwards, iPLNPs were administered to Ai9 mice via i.v. injection. PBS group was used as negative control. After 10 d, mice were killed and the organs were isolated and imaged on the IVIS Spectrum in vivo imaging system (Perkin Elmer). Then, tissues were embedded in optimal cutting temperature compound and cut into 10 µm sections. After fixing with 4% paraformaldehyde for 20 min, the sections were washed three times with PBS. Afterward, ProLong Gold Mountant with 4,6-diamidino-2-phenylindole was dropped to the slides, and coverslips were covered. These slides were imaged by confocal microscopy (Zeiss LSM 700), and analysed with ZEN 2010 software v.6.0.62 (Carl Zeiss MicroImaging).

In vivo codelivery of Cas9 mRNA and sgPTEN for gene editing. PTEN was selected to examine endogenous gene editing in vivo. iPLNPs containing Cas9 mRNA and modified sgPTEN (mRNA to sgRNA weight ratio of 4 to 1, total

RNA dose 0.75 mg kg⁻¹) were prepared as in vivo iPLNP formulation method mentioned above. 9A1P9:5A2-SC8:cholesterol:DMG-PEG2000 (molar ratio) of 25:30:30:1 and 9A1P9:DDAB:cholesterol:DMG-PEG2000 (molar ratio) of 60:30:40:0.4 were used for 9A1P9-5A2-SC8 iPLNP and 9A1P9-DDAB iPLNP, respectively. The 9A1P9 to RNA weight ratio was fixed at 18 to 1. Afterwards, iPLNPs were administered to wild type C57BL/6 mice (6–8 weeks old) via i.v. injection. Ten days later, tissues were collected and genomic DNA was extracted with a PureLink Genomic DNA Mini Kit (Thermo Fisher). Post obtainment of PTEN PCR products (Supplementary Table 3), the T7E1 assay was used to measure the gene editing efficacy by the standard protocol (NEB) (Supplementary Fig. 27). Furthermore, gene editing efficacy of PTEN was evaluated by Image J (1.50b Java 1.8.0_60 (64-bit), National Institutes of Health). Indel (%) is calculated as $100 \times (1 - (1 - \text{fraction cleaved})^{0.5})$, where the fraction cleaved is defined as (Fragment 1 + Fragment 2)/(Fragment 1 + Fragment 2 + Parent Fragment).

Statistical analyses. Statistical analyses were performed using GraphPad Prism v.8 (GraphPad Software). A two-tailed unpaired Student's *t*-test was used to determine the significance of the indicated comparisons. Data are expressed as mean \pm s.d. *P* values <0.05 (*), *P*<0.01 (**), *P*<0.001 (***) and *P*<0.0001 (****) were considered to be statistically significant.

Reporting Summary. Further information on research design is available in the Nature Research Reporting Summary linked to this article.

Data availability

All relevant data supporting the findings of this study are available within the paper and Supplementary Information. The raw data is available from the corresponding author upon request.

Acknowledgements

D.J.S. acknowledges financial support from the National Institutes of Health (NIH) National Institute of Biomedical Imaging and Bioengineering (NIBIB) (grant no. R01 EB025192-01A1), the American Cancer Society (ACS) (grant no. RSG-17-012-01), the Welch Foundation (grant no. I-1855) and the Cystic Fibrosis Foundation (CFF) (grant no. SIEGWA18XXO). T.W. acknowledges financial support from the Cancer Prevention and Research Institute of Texas (CPRIT) Training grant (no. RP160157). We acknowledge the UTSW Tissue Resource, supported in part by the National Cancer Institute (grant no. 5P30CA142543) and the Moody Foundation Flow Cytometry Facility.

Author contributions

S.L., Q.C. and D.J.S. designed the research. S.L., Q.C., T.W., X.Y., L.T.J. and L.F. performed the experiments. All the authors were involved in the data analyses. S.L. and D.J.S. wrote the manuscript, and all authors discussed and commented on it. D.J.S. directed the research.

Competing interests

D.J.S., S.L., Q.C., T.W. and X.Y., and the Reagents of the University of Texas System have filed a patent application on this technology.

Additional information

Supplementary information is available for this paper at <https://doi.org/10.1038/s41563-020-00886-0>.

Correspondence and requests for materials should be addressed to D.J.S.

Peer review information *Nature Materials* thanks Bruno Pitard, John Rossi and the other, anonymous, reviewer(s) for their contribution to the peer review of this work.

Reprints and permissions information is available at www.nature.com/reprints.

Corresponding author(s): Daniel J. Siegwart

Last updated by author(s): Oct 2, 2020

Reporting Summary

Nature Research wishes to improve the reproducibility of the work that we publish. This form provides structure for consistency and transparency in reporting. For further information on Nature Research policies, see [Authors & Referees](#) and the [Editorial Policy Checklist](#).

Statistics

For all statistical analyses, confirm that the following items are present in the figure legend, table legend, main text, or Methods section.

n/a Confirmed

- The exact sample size (n) for each experimental group/condition, given as a discrete number and unit of measurement
- A statement on whether measurements were taken from distinct samples or whether the same sample was measured repeatedly
- The statistical test(s) used AND whether they are one- or two-sided
Only common tests should be described solely by name; describe more complex techniques in the Methods section.
- A description of all covariates tested
- A description of any assumptions or corrections, such as tests of normality and adjustment for multiple comparisons
- A full description of the statistical parameters including central tendency (e.g. means) or other basic estimates (e.g. regression coefficient) AND variation (e.g. standard deviation) or associated estimates of uncertainty (e.g. confidence intervals)
- For null hypothesis testing, the test statistic (e.g. F , t , r) with confidence intervals, effect sizes, degrees of freedom and P value noted
Give P values as exact values whenever suitable.
- For Bayesian analysis, information on the choice of priors and Markov chain Monte Carlo settings
- For hierarchical and complex designs, identification of the appropriate level for tests and full reporting of outcomes
- Estimates of effect sizes (e.g. Cohen's d , Pearson's r), indicating how they were calculated

Our web collection on [statistics for biologists](#) contains articles on many of the points above.

Software and code

Policy information about [availability of computer code](#)

Data collection

Zetasizer software version 7.13 (Malvern Panalytical)
ZEN x64 software version 1.1.0 (Carl Zeiss Microscopy GmbH)
Living Image software version 4.3 (64-bit, Caliper Life Sciences)
BD FACSDiva software version 8.0.1 (BD LSRIFortessa)
NDP.scan software version 3.1.9 (NANOZOOMER, Hamamatsu)

Data analysis

ZEN 2010 software version 6.0.62 (Carl Zeiss MicroImaging GmbH)
GraphPad Prism 8 software version 8.3.0 (GraphPad Software)
Living Image software version 4.3 (64-bit, Caliper Life Sciences)
FLOWJO software version 7.6 (FLOWJO)
NDP.view 2 software version 2.7.25 (Hamamatsu)
Image J 1.50b Java 1.8.0_60 (64-bit) (National Institutes of Health, USA)

For manuscripts utilizing custom algorithms or software that are central to the research but not yet described in published literature, software must be made available to editors/reviewers. We strongly encourage code deposition in a community repository (e.g. GitHub). See the Nature Research [guidelines for submitting code & software](#) for further information.

Data

Policy information about [availability of data](#)

All manuscripts must include a [data availability statement](#). This statement should provide the following information, where applicable:

- Accession codes, unique identifiers, or web links for publicly available datasets
- A list of figures that have associated raw data
- A description of any restrictions on data availability

The authors declare that all data supporting the findings of this study are available within the paper [and its supplementary information files].

The data that support the findings of this study are available from the corresponding author upon reasonable request.

Field-specific reporting

Please select the one below that is the best fit for your research. If you are not sure, read the appropriate sections before making your selection.

Life sciences Behavioural & social sciences Ecological, evolutionary & environmental sciences

For a reference copy of the document with all sections, see nature.com/documents/nr-reporting-summary-flat.pdf

Life sciences study design

All studies must disclose on these points even when the disclosure is negative.

| | |
|-----------------|--|
| Sample size | Power analysis was employed to determine sample sizes. |
| Data exclusions | No data were excluded. |
| Replication | Reported results were consistently replicated across multiple experiments with all replicates generating similar results. We have used C57BL/6 mice and tdTomato reporter mice (Ai9 mice) mice to confirm organ selective mRNA delivery and gene editing in lung, spleen, or liver. The narrow variations also confirmed that our experimental findings are reproducible. Key data generated by one co-author were repeated by other co-authors independently. |
| Randomization | No randomization was necessary for cell based experiments because investigators were comparing nanoformulations under well controlled conditions. For animal experiments, mice with ages of 6-8 weeks were randomly allocated into each treatment group. |
| Blinding | Due to the proof-of-concept developmental nature of this study, true blinding of experiments was not performed. However, data collection and analyses for some experiments were performed by separate individuals. In some cases, these collectors/analyzers were not aware which samples corresponded to which experimental groups at the time of data collection and analysis. |

Reporting for specific materials, systems and methods

We require information from authors about some types of materials, experimental systems and methods used in many studies. Here, indicate whether each material, system or method listed is relevant to your study. If you are not sure if a list item applies to your research, read the appropriate section before selecting a response.

Materials & experimental systems

- | | |
|-------------------------------------|---|
| n/a | Involved in the study |
| <input type="checkbox"/> | <input checked="" type="checkbox"/> Antibodies |
| <input type="checkbox"/> | <input checked="" type="checkbox"/> Eukaryotic cell lines |
| <input checked="" type="checkbox"/> | <input type="checkbox"/> Palaeontology |
| <input type="checkbox"/> | <input checked="" type="checkbox"/> Animals and other organisms |
| <input checked="" type="checkbox"/> | <input type="checkbox"/> Human research participants |
| <input checked="" type="checkbox"/> | <input type="checkbox"/> Clinical data |

Methods

- | | |
|-------------------------------------|--|
| n/a | Involved in the study |
| <input checked="" type="checkbox"/> | <input type="checkbox"/> ChIP-seq |
| <input type="checkbox"/> | <input checked="" type="checkbox"/> Flow cytometry |
| <input checked="" type="checkbox"/> | <input type="checkbox"/> MRI-based neuroimaging |

Antibodies

Antibodies used

We used multiple monoclonal antibodies in the flow cytometry to determine tissue specific editing by Cre mRNA in tdTomato mice in Fig. S25-S26. These antibodies are: Pacific Blue anti-mouse CD45 (BioLegend, 103126), Alexa Fluor 488 anti-mouse/human CD11b (BioLegend, 101217), Alexa Fluor 647 anti-mouse CD19 (BioLegend, 115522), PerCP-Cyanine5.5 Anti-Mouse CD3e (145-2C11) (Tonbo Biosciences, 65-0031), Alexa Fluor 488 anti-mouse CD31 (BioLegend, 102414) and Alexa Fluor 647 anti-mouse CD326 (Ep-CAM) (BioLegend, 118212).

Validation

1. The Pacific Blue anti-mouse CD45 has been validated to be used for immunofluorescent staining with flow cytometric analysis. The suggested use of this reagent is $\leq 0.25 \mu\text{g}$ per million cells in $100 \mu\text{l}$ volume from the manufacturer's website and it is also mentioned species reactivity with mouse thymus or spleen. (<https://www.biologend.com/en-us/products/pacific-blue-anti-mouse-cd45 antibody-3102>). After titration, we finally used 1/400 dilution for lung cell types and 1/200 dilution for spleen.
2. Alexa Fluor 488 anti-mouse/human CD11b has been validated to be used for immunofluorescent staining with flow cytometric analysis. The suggested use of this reagent is $\leq 0.25 \mu\text{g}$ per million cells in $100 \mu\text{l}$ volume from the manufacturer's website and it is also mentioned species reactivity with C57BL/10 splenocytes. (<https://www.biologend.com/en-us/products/alexa-fluor-488-anti-mouse-human-cd11b antibody-2700>). After titration, we finally used 1/1600 dilution for analysis.
3. Alexa Fluor 647 anti-mouse CD19 has been validated to be used for immunofluorescent staining with flow cytometric analysis. The suggested use of this reagent is $\leq 0.25 \mu\text{g}$ per million cells in $100 \mu\text{l}$ volume from the manufacturer's website and it is also mentioned species reactivity with Mouse CD19-expressing K562 human erythroleukemia cells. (<https://www.biologend.com/en-us/products/alexa-fluor-647-anti-mouse-cd19 antibody-2705>). After titration, we finally used 1/400 dilution for analysis.
4. PerCP-Cyanine5.5 Anti-Mouse CD3e (145-2C11), has been validated to be used for immunofluorescent staining with flow

cytometric analysis and mentioned species reactivity with mouse. (<https://tonbobio.com/products/percp-cyanine5-5-anti-mouse-cd3e-145-2c11>). After titration, we finally used 1/40 dilution for analysis.

5. Alexa Fluor 488 anti-mouse CD31 has been validated to be used for immunofluorescent staining with flow cytometric analysis. The suggested use of this reagent is $\leq 0.25 \mu\text{g}$ per million cells in 100 μl volume from the manufacturer's website and it is also mentioned species reactivity with C3H/HeJ mouse hematopoietic progenitor cell line 3. (<https://www.biologend.com/en-us/products/alex-fluor-488-anti-mouse-cd31-antibody-3091>). After titration, we finally used 1/800 dilution for analysis.

6. Alexa Fluor 647 anti-mouse CD326 (Ep-CAM) has been validated to be used for immunofluorescent staining with flow cytometric analysis. The suggested use of this reagent is $\leq 0.25 \mu\text{g}$ per million cells in 100 μl volume from the manufacturer's website and it is also mentioned species reactivity with TE-71 thymic epithelial cell line. (<https://www.biologend.com/en-us/products/alex-fluor-647-anti-mouse-cd326-ep-cam-antibody-4973>). After titration, we finally used 1/1600 dilution for analysis.

Eukaryotic cell lines

Policy information about [cell lines](#)

| | |
|--|--|
| Cell line source(s) | IGROV1 and Hela cells were originally obtained from ATCC. Derived HeLa-Luc reporter cells were generated using lentiviruses from HeLa cells originally obtained from ATCC. |
| Authentication | The cell lines were not further authenticated after receiving from ATCC. |
| Mycoplasma contamination | The cell lines were not tested for mycoplasma contamination. |
| Commonly misidentified lines (See ICLAC register) | No commonly misidentified cell lines were used. |

Animals and other organisms

Policy information about [studies involving animals](#); [ARRIVE guidelines](#) recommended for reporting animal research

| | |
|-------------------------|---|
| Laboratory animals | Mice were maintained in a barrier facility with a 12-h light/12-h dark cycle, at 20 ~ 26 °C (average 22 °C) and 30% ~ 60% humidity (average 50%). C57BL/6 mice were obtained from the UTSW Mouse Breeding Core Facility. Male and female mice with age of 6-8 weeks were used. B6.Cg-Gt(ROSA)26Sortm9(CAGtdTomato)Hze/J mice (also known as Ai9 or Ai9(RCL-tdT) mice) were obtained from The Jackson Laboratory (007909) and bred to maintain homozygous expression of the Cre reporter allele that has a loxP-flanked STOP cassette preventing transcription of a CAG promoter-driven red fluorescent tdTomato protein. Following Cre-mediated recombination or CRISPR/Cas9 based gene editing, Ai9 mice will express tdTomato fluorescence. Ai9 mice are congenic on the C57BL/6J genetic background. Ai9 female mice with ages of 6-8 weeks were used. |
| Wild animals | The study did not involve wild animals. |
| Field-collected samples | The study did not involve samples collected from the field. |
| Ethics oversight | All animal experiments were approved by the Institution Animal Care and Use Committees of The University of Texas Southwestern Medical Center and were consistent with local, state and federal regulations as applicable. |

Note that full information on the approval of the study protocol must also be provided in the manuscript.

Flow Cytometry

Plots

Confirm that:

- The axis labels state the marker and fluorochrome used (e.g. CD4-FITC).
- The axis scales are clearly visible. Include numbers along axes only for bottom left plot of group (a 'group' is an analysis of identical markers).
- All plots are contour plots with outliers or pseudocolor plots.
- A numerical value for number of cells or percentage (with statistics) is provided.

Methodology

| | |
|--------------------|--|
| Sample preparation | Hepatocytes were isolated using a two-step collagenase perfusion. The mice were anesthetized by isoflurane and fixed. Then perfusion was performed with liver perfusion medium (Thermo Fisher, 17701038) for 7-10 min, and followed by liver digestion medium (Thermo Fisher, 17703034) for another 7-10 min. Liver was cut to release the hepatocytes in liver digestion medium (10 mL), and the hepatocytes were washed with cold hepatocyte wash medium (Thermo Fisher, 17704024) and collected by centrifugation (low speed, 50 g, 5 min). The cell pellet was resuspended in cold hepatocyte wash medium, and passed through a 100 μm filter. Then, the hepatocytes were washed twice more using cold hepatocyte wash medium, once with 1X PBS and passed through the 100 μm filter again. The hepatocytes were collected by centrifugation (50 g, 5 min), and analyzed with the fluorescence-activated cell sorting (FACS) Aria II SORP machine (BD FACSDiva software version 8.0.1, BD Biosciences). For spleen cell isolation and staining, the collected spleen was minced and homogenized in 1X digestion medium (250 μL , 45 units μL^{-1} collagenase I, 25 units μL^{-1} DNase I and 30 units μL^{-1} hyaluronidase). The mixture was transferred to a 15 ml tube containing 1X digestion medium (10 mL). Then the mixture was passed through a 70 μm filter and washed with 1X PBS. After centrifugation (300 g, 5 min, 4 °C), the cells were collected. Afterward, the cells were resuspended in 1X red blood cell lysis |
|--------------------|--|

buffer (2 mL, BioLegend, 420301) and incubated on ice for 5 min. Cell staining buffer (4 mL, BioLegend) was then added to stop the red blood cell lysis. The mixture was centrifuged (300 g, 5 min) and the obtained pellet was resuspended in cell staining buffer. The cells and antibodies were transferred to flow tubes (100 µL), following incubation for 20 min at 4 °C in the dark. Then the cells were washed twice using 1X PBS, and resuspended in 1X PBS (500 µL) for final analysis. The antibodies, Alexa Fluor 488 anti-mouse/human CD11b (1/1600 dilution, BioLegend, 101217), Pacific Blue anti-mouse CD45 (1/200 dilution, BioLegend, 103126), PerCP-Cyanine5.5 anti-mouse CD3e (145-2C11) (1/40 dilution, Tonbo Biosciences, 65-0031) and Alexa Fluor 647 anti-mouse CD19 (1/400 dilution, BioLegend, 115522) were used here. Ghost Dye Red 780 (Tonbo Biosciences, 13-0865-T500) was utilized to discriminate live cells. Ultimately, the spleen cells were analyzed with the LSRFortessa SORP machine (BD Biosciences). For lung cell isolation and staining, the collected lung was minced and added in a 15 ml tube containing 2X digestion medium (10 mL, 90 units µL⁻¹ collagenase I, 50 units µL⁻¹ DNase I and 60 units µL⁻¹ hyaluronidase). The mixture was incubated for 1 h at 37 °C under shaking. Afterward, the remaining lung tissue was homogenized. The remaining procedures were the same as above spleen protocol. The antibodies, Alexa Fluor 488 anti-mouse CD31 (1/800 dilution, BioLegend, 102414), Pacific Blue anti-mouse CD45 (1/400 dilution, BioLegend, 103126) and Alexa Fluor 647 anti-mouse CD326 (Ep-CAM) (1/1600 dilution, BioLegend, 118212) were used here. Ghost Dye Red 780 was utilized to discriminate live cells. Ultimately, the lung cells were analyzed with above LSRFortessa SORP machine. These data were analyzed with FLOWJO software version 7.6 (FLOWJO).

Instrument

FACS Aria II SORP (BD Biosciences) and LSRFortessa SORP (BD Biosciences)

Software

Data collection: BD FACSDiva software version 8.0.1 (BD LSRFortessa);
Data analysis: FLOWJO software version 7.6 (FLOWJO)

Cell population abundance

We used tdTomato (A19) mice to evaluate tissue specific gene editing efficiency (Cre mediated) via detecting the tdTomato mean fluorescence intensity.

Gating strategy

Gates for Td-Tom+ in cell types were drawn based on control mice. Gating strategy were provided in SI Figures.

Tick this box to confirm that a figure exemplifying the gating strategy is provided in the Supplementary Information.